PL-CP--93-1001

Published in:
Proc. 7th International Cryocooler Conference
17-19 November, 1992
Air Force Report PL-CP-93-1001, April 1993
pp. 783-804

DESIGN EQUATIONS AND SCALING LAWS FOR LINEAR COMPRESSORS WITH FLEXURE SPRINGS*

Eric Marquardt and Ray Radebaugh
National Institute of Standards and Technology
Boulder, CO 80303

Peter Kittel
NASA/Ames Research Center
Moffett Field, CA 94035

ABSTRACT

Linear-resonant compressors with flexure springs and clearance seals have recently been developed for use in long-life Stirling and pulse tube refrigerators. This paper describes a set of equations that are used to design the various components in the compressor given specified performance criteria. The components considered are the moving-coil linear motor, the mass of the moving components, the magnet assembly, the flexure springs, and the clearance seals. Both radially and axially magnetized magnets are analyzed and the criteria for selection are developed. Methods for reducing the compressor size and mass are discussed as well as the influence of the stroke-to-diameter ratio on the design of flexure springs. The design equations have allowed the development of scaling laws for linear motor compressors covering a wide range of compressor sizes from 3 watts to 4 kilowatts.

INTRODUCTION

This paper develops a set of equations for the geometrical parameters of a linear motor compressor in terms of the performance parameters. These equations then show how the dimensions are affected by the specified performance parameters. Figure 1 shows a schematic of a simple reciprocating compressor with a linear motor drive. The axial direction is parallel to the center line (defined here as the z axis), and the radial direction is perpendicular to the center line. These compressors use a current carrying wire (and thus, are called a moving coil design) within a magnetic field to impart a linear force in the axial direction to the piston while

*Research sponsored by NASA/Ames Research Center. Contribution of NIST, not subject to copyright.

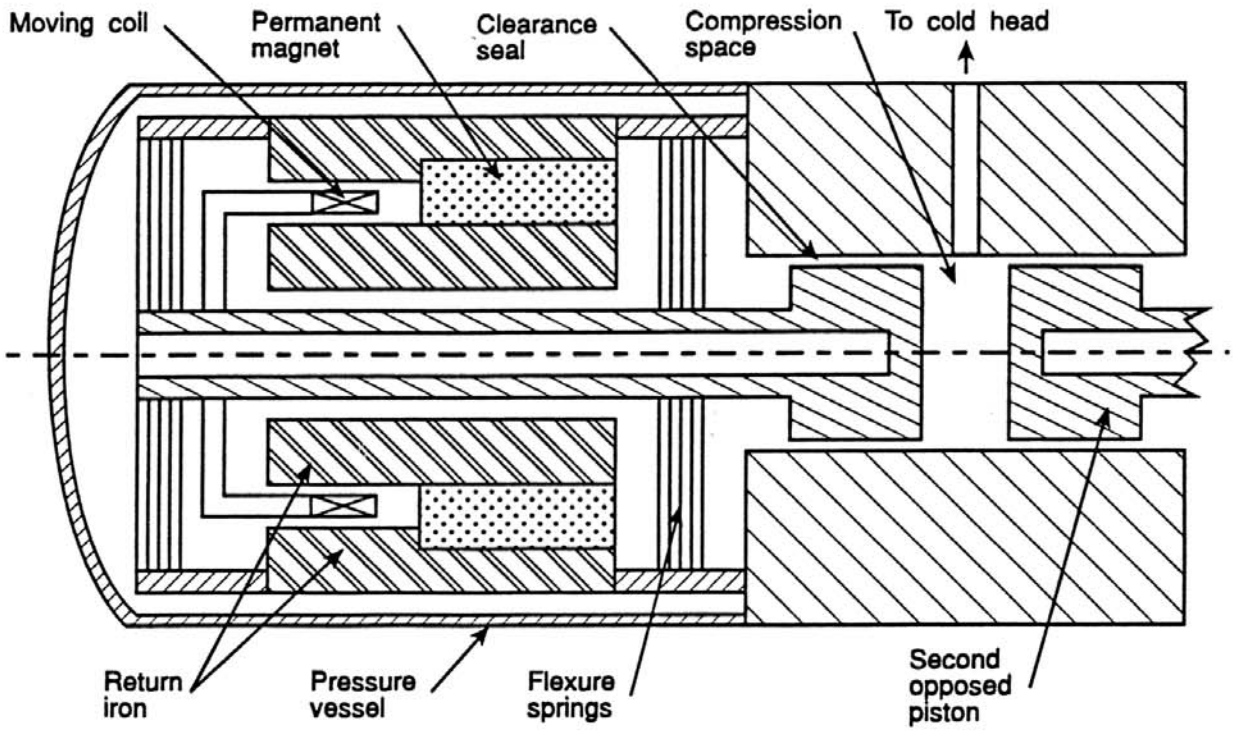

Figure 1. Schematic of a linear motor compressor. The drawing is axisymmetric about the dashed center line.

conventional rotary compressors use a crank shaft to provide this force. Rotary compressors apply large radial forces to the piston, which provide no useful work, cause a large amount of wear, and usually require lubrication. Lubrication is a problem in cryocoolers since contaminant can often migrate to the cold end of the refrigerator and liquefy or freeze. Linear motors eliminate radial forces completely since the force created in the wire is perpendicular to both the magnetic field and the direction of the current in the wire.[1] A linear motor compressor can operate at any frequency but is most efficient operating at a unique resonant frequency, usually in the range of 30 to 60 Hz.

Vibration of reciprocating compressors can be reduced by using a balanced-opposed design. In this configuration, the pistons are counter-balanced in-line, 180° out of phase, as shown in Figure 1. Traditionally the seal between the piston and cylinder has been accomplished using piston rings and is another source of wear in the compressor. Clearance seals can achieve the same effect while eliminating contact between the piston and cylinder wall, thus eliminating wear. A gap generally on the order of 15 μm is used and allows only a small percentage of the working fluid to pass through during a half cycle. The gas pressure on the backside of the piston is the average of that in the compression space, so there is no loss of gas from the compression space when averaged over one cycle. Clearance seals require very good alignment between the

piston and cylinder over the entire stroke. Traditional sliding bearings could be used to achieve this alignment, but there will be wear in the bearings and the alignment will be lost over time. Magnetic bearings could also be used but are large and complex. Flexure springs address this problem since they have no rubbing parts and are simple to construct. The flexure spring is constructed from a thin flexible material and is much stiffer in the radial direction than in the axial direction. They were first used in a Stirling refrigerator at the University of Oxford.[2]

The design of a linear motor compressor generally begins by specifying the performance parameters. These parameters are: (1) the required PV power $\dot{W}_{PV}$, (2) the desired efficiency of conversion of electrical power to PV power η, (3) the operating frequency f, (4) the average system pressure P_0, (5) the pressure ratio P_r, defined as the maximum pressure over the minimum pressure, and (6) the phase angle ϕ by which the pressure leads the piston position. In some cases the compressor swept volume V_{co}, may be used as an input parameter in place of the PV power. The compressor geometry, such as the stroke, clearance gap, coil dimensions, magnet configuration, return iron dimensions, and flexure spring dimensions must be optimized to give the minimum weight and/or system size that provides the specified performance parameters.

PHASOR ANALYSIS

Phasor analysis allows us to write simple algebraic equations in place of differential equations when solving sinusoidal steady-state problems.[3] A phasor is a complex number expressed in polar coordinates as $\mathbf{v} = V_0 e^{i(\omega t+\phi)}$ and whose projection on the real axis describes the sinusoid $v(t) = V_0\cos(\omega t+\phi)$. The phasor $\mathbf{v}$ is represented by an arrow of length $|\mathbf{v}|=V_0$ and an angle ϕ measured counterclockwise from the positive real axis at time $t=0$. The rotation of this phasor about the origin in a counterclockwise direction with angular frequency ω describes the time dependance of the phasor. It is necessary to show the phasors only at $t=0$, since all phasors for a linear system have the same frequency. Such a visual display is clearer than showing many time dependent sinusoids. The time derivative of a phasor is given as

$$\frac{d}{dt} V_0 e^{i(\omega t+\phi)} = i\omega V_0 e^{i(\omega t+\phi)}. \tag{1}$$

Since $i = e^{i\pi/2}$, we can write the derivative as

$$\dot{\mathbf{v}} = \omega V_0 e^{i(\omega t+\phi)} e^{i\pi/2} = \omega V_0 e^{i(\omega t+\phi+\pi/2)}. \tag{2}$$

Equation (2) shows that the time derivative of a sinusoid leads the original sinusoid by $\pi/2$ radians or 90°. Phasors may be treated the same as vectors, but they are in complex space instead of real space. We represent phasors in this paper with bold variables.

Phasor analysis is useful for regenerative cryocoolers, such as Stirling and pulse tube refrigerators, because of the nearly sinusoidal variations of volume, pressure, mass flow, and temperature. Phasors are used here to represent all the forces acting on the sinusoidally driven piston of the compressor. The driving force F_{LM} that must be supplied by the moving coil of the linear motor is given by the force balance

$$\begin{aligned} F_{LM} &= m\ddot{z} + b\dot{z} + k_z z + PA - P_B A \\ &= F_I + F_{vd} + F_s + F_P - F_B , \end{aligned} \tag{3}$$

where z is the position of the piston from its midpoint (positive numbers toward smaller compressor volume), m is the mass of the moving piston and coil assembly, b is the dissipation constant that gives rise to viscous losses, k_z is the flexure spring stiffness in the z direction, P is the dynamic pressure in the compression space, P_B is the dynamic pressure on the backside of the piston, and A is the piston cross-sectional area. Let the position phasor be given by

$$z = (s/2)e^{i\omega t}, \tag{4}$$

where s is the piston stroke and the phase angle of this reference phasor is made zero. The dynamic pressure in the working space P and in the backside P_B are given by

$$P = P_1 e^{i(\omega t+\phi)}, \tag{5}$$

$$-P_B = P_{B1} e^{i(\omega t+\beta)}, \tag{6}$$

where P_1 and P_{B1} are the amplitudes of the dynamic pressures with phase angles of ϕ and β respectively. Note that β refers to the negative of P_B. The resulting force balance from Eq. (3) is represented by phasors in Fig. 2. The magnitudes of the phasors are given by

$$\begin{aligned} |F_{LM}| &= L_w I B, \\ |F_s| &= \tfrac{1}{2} k_z s, \\ |F_B| &= P_{B1} A, \\ |F_P| &= P_1 A, \\ |F_{vd}| &= \pi f s b, \\ |F_I| &= 2\pi^2 f^2 s m, \end{aligned} \tag{7}$$

where F_{LM} is the linear motor force, F_s is the mechanical spring force, F_{vd} is the viscous dissipation, and F_I is the inertial force. The phase angle of F_s is 0° because it is in phase with the position. The phase angle for F_{vd} is 90° since it is in phase with $\dot{z}$. The phase angle for F_I is 180° since it is in phase with $\ddot{z}$. The phase angle ϕ will depend on the particular cold head attached to the compressor. A typical value based on experiments may be about 35° to 40° for a pulse tube and about 40° to 45° for a Stirling refrigerator. Accurate values of this phase angle are needed for the proper design of the compressor. In most practical compressors, the volume

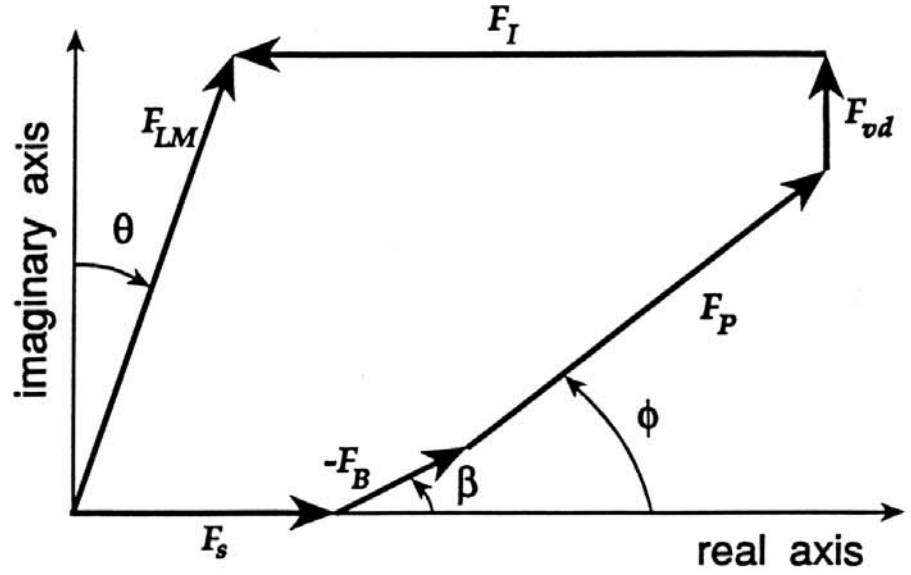

Figure 2. Phasor diagram showing the forces acting on the piston.

of the gas on the backside of the piston is much larger than that of the compression space. As a result F_B is negligible. Also the velocity of the moving components is usually small enough that the viscous dissipation term $b\dot{z}$ is negligible compared to the pressure term. The flow through the clearance gap results in a loss of some of the piston PV work that never reaches the cold head, however it has a negligible effect on the force balance. Figure 3 shows the phasor diagram without the backside pressure and viscous dissipation phasors. The relative magnitudes and phase angles are typical of most compressors, except θ may be zero or even slightly negative in some cases. Figure 3 shows that the motor force is minimized by adjusting m to make θ=0. This condition is defined as resonance, which occurs when the inertial force is balanced by the sum of the real parts of the mechanical and gas spring forces. Since the motor force varies as (1/cosθ), θ can be increased to ±20° with only a 6.4% increase in the motor force. For positive θ (F_{LM} lagging $\dot{z}$) the moving mass can be reduced, which reduces the vibration effects.

DESIGN EQUATIONS

Moving Mass

To operate the compressor at a predetermined frequency, it is necessary to determine the moving mass needed to achieve a resonant or near resonant condition. The moving mass is the entire piston assembly including the piston, piston shaft, coil, coil holder, and a portion of the flexure spring mass. To calculate the moving mass, the forces in Figure 3 are balanced in the real direction to give

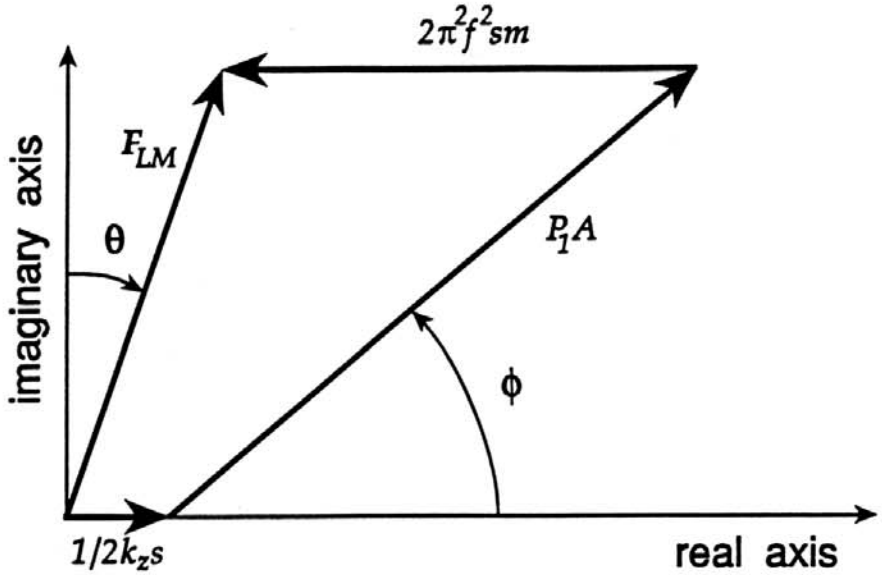

Figure 3. Phasor diagram used for the force balance on the piston.

$$|F_{LM}|\sin\theta + 2\pi^2 f^2 sm = \tfrac{1}{2}k_z s + P_1 A\cos\phi. \tag{8}$$

The area of the piston A is expressed in more fundamental parameters as

$$A = V_{co}/s, \tag{9}$$

where V_{co} is the compressor swept volume and is to be regarded here as a specified parameter. The amplitude of the dynamic pressure is best expressed in the form of two components as

$$P_1 = (P_1/P_0)P_0, \tag{10}$$

where (P_1/P_0) is related to the pressure ratio P_r by

$$P_1/P_0 = \frac{P_r - 1}{P_r + 1}. \tag{11}$$

The motor force F_{LM} is calculated from a force balance along the imaginary axis in Figure 3,

$$|F_{LM}|\cos\theta = P_1(V_{co}/s)\sin\phi. \tag{12}$$

The term $|F_{LM}|$ from Eq. (12) is substituted into Eq. (8) and the moving mass is found to be

$$m = \frac{\frac{1}{2}k_z s + (P_1/P_0)P_0(V_{co}/s)\cos\phi(1 - \tan\phi\tan\theta)}{2\pi^2 s f^2}. \tag{13}$$

Compressor Power

The instantaneous PV power $\dot{W}_{PV}$ produced by the compressor is given as

$$\dot{W}_{PV} = -P\dot{V}_{co}, \tag{14}$$

where $\dot{V}_{co}$ is the time rate of change of the compressor volume. The time-averaged PV power $<\dot{W}_{PV}>$ is given by

$$<\dot{W}_{PV}> = -\tfrac{1}{2}Re[P\dot{V}_{co}^{*}] = \tfrac{1}{2}Re[P_1 e^{i\phi}|\dot{V}_{co}|e^{-i\pi/2}] = \tfrac{1}{2}P_1|\dot{V}_{co}|\sin\phi, \tag{15}$$

where $\dot{V}_{co}^{*}$ is the complex conjugate of $\dot{V}_{co}$ and Re[ ] denotes the real part of the argument. In a simpler manner using phasors, the time-averaged PV power is given by

$$<\dot{W}_{PV}> = -\tfrac{1}{2}\boldsymbol{P}\cdot\dot{\boldsymbol{V}}_{co} = \tfrac{1}{2}P_1|\dot{V}_{co}|\cos\alpha, \tag{16}$$

where the dot product treats the phasors as vectors and α is the phase angle between $\boldsymbol{P}$ and $-\dot{\boldsymbol{V}}_{co}$. Because $\alpha = \pi/2-\phi$, Eq. (16) becomes

$$<\dot{W}_{PV}> = \tfrac{1}{2}P_1|\dot{V}_{co}|\sin\phi, \tag{17}$$

which is the same as Eq. (15). Because $|\dot{V}_{co}| = 2\pi f(V_{co}/2)$, the time-averaged PV power can be expressed as

$$<\dot{W}_{PV}> = (\pi/2)fP_1V_{co}\sin\phi. \tag{18}$$

Equation (18) is used to interchange input parameters between V_{co} and $<\dot{W}_{PV}>$ in the design equations.

Clearance Seal

The gap thickness for the clearance seal must be made sufficiently small to keep the amplitude of the flow rate through the gap small compared with the amplitude of the flow rate between the compressor and the cold head. The PV work lost through the gap should be small compared with the total PV work delivered by the piston. Flow through the narrow gap is always laminar. Thus, the flow impedance Z_f of the gap is a function only of the gap geometry and can be expressed as[4]

$$Z_f = \frac{\Delta P}{\mu \dot{V}_{cg}} = \frac{12 L_{cg}}{w t_g^3}, \tag{19}$$

where ΔP is the pressure drop across the gap, μ is the viscosity, $\dot{V}_{cg}$ is the volume flow rate through the gap, L_{cg} is the gap length, w is the gap width, and t_g is the gap thickness. Because of the proportionality between ΔP and $\dot{V}_{cg}$, the amplitudes can be used for these two quantities instead of the instantaneous values. The dynamic pressure amplitude P_1 is equal to $|\Delta P|$ and the amplitude of $\dot{V}_{cg}$ can be expressed as $\dot{V}_{cg}=|\dot{V}_{cg}||\dot{V}_{co}|/|\dot{V}_{co}|$ where $|\dot{V}_{co}|=2\pi f(V_{co}/2)$. The gap width is expressed as $w=\pi D=2\sqrt{(\pi V_{co}/s)}$ for an annular gap. Substituting these terms into Eq. (19) and solving for the clearance gap thickness t_g gives

$$t_g = \left[\frac{6\mu L_{cg} f(|\dot{V}_{cg}|/|\dot{V}_{co}|)\sqrt{\pi s V_{co}}}{(P_1/P_0)P_0} \right]^{\frac{1}{3}}. \tag{20}$$

The time-averaged PV power loss due to flow through the gap is $<\dot{W}_g> = \frac{1}{2}\boldsymbol{P}\cdot\dot{\boldsymbol{V}}_{cg} = \frac{1}{2}P_1|\dot{V}_{cg}|\cos\beta$, where β is the angle between $\dot{V}_{cg}$ and $\boldsymbol{P}$, which is 0 from Eq. (19), leading to

$$<\dot{W}_g> = \tfrac{1}{2}P_1|\dot{V}_{cg}|. \tag{21}$$

Substituting Eqs. (21) and (17) into Eq. (20) yields

$$t_g = \left[\frac{6\mu L_{cg} f(<\dot{W}_g>/<\dot{W}_{PV}>)\sqrt{\pi s V_{co}}\,\sin\phi}{(P_1/P_0)P_0} \right]^{\frac{1}{3}}, \tag{22}$$

where $<\dot{W}_g>/<\dot{W}_{PV}>$ is the fraction of PV power lost to flow through the gap. Equations (20) and (22) are valid for a uniform gap. If the piston is not concentric with the cylinder, the flow loss can be significantly higher since the flow is proportional to t_g^3 according to Eq. (19).

Linear Motor

A linear motor can be made with a moving coil, moving magnet, or moving iron. Kerney[5] compares these three types of linear motors. Because of its low weight, high efficiency, and zero radial forces, the moving coil motor is the one most often used for space applications of cryocoolers. With the moving coil motor, the magnet can be magnetized in either the radial or axial directions as shown in Figure 4. In order for a sinusoidal current in the coil to produce a sinusoidal force, the coil must be in a uniform magnetic field. The coil can be made short and

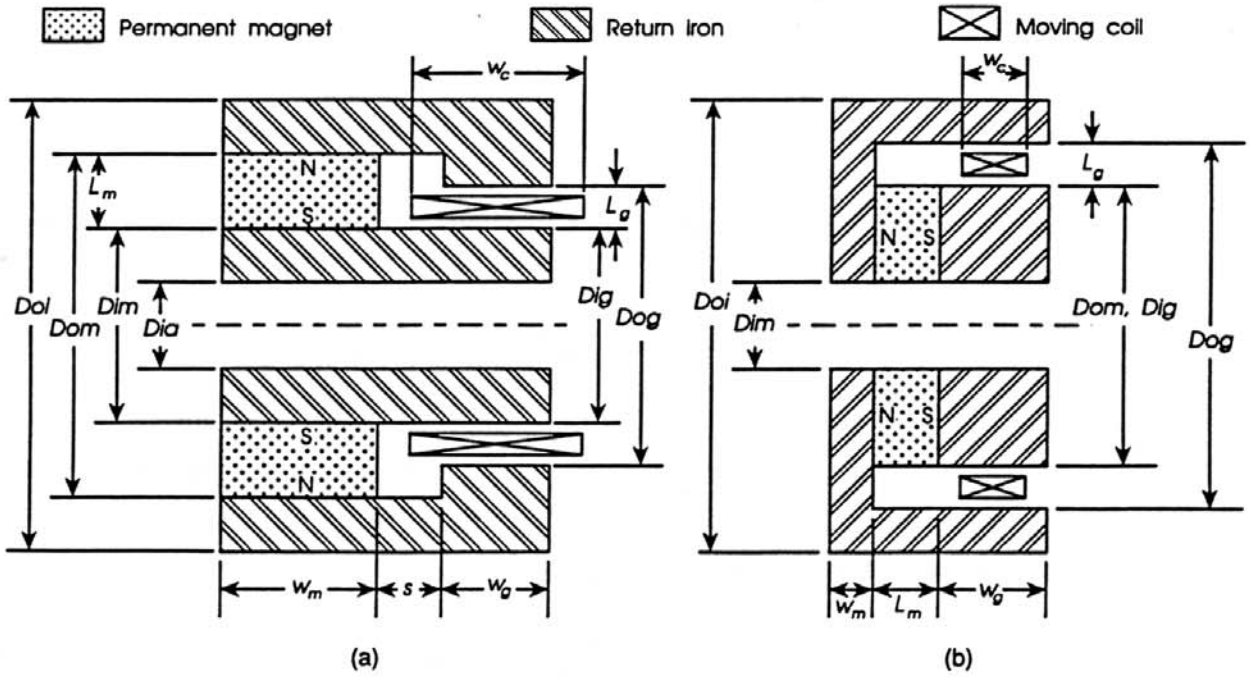

Figure 4. Geometry for (a) radial magnet and (b) axial magnet.

remain in the uniform magnetic field for the entire stroke (short coil as shown in Figure 4b) or a fixed magnetic field may remain within the coil for the entire stroke (long coil as shown in Figure 4a).

First the short coil design is discussed. The first step is to calculate the coil volume V_c, which is the volume of wire needed to produce the desired force including any insulation or epoxy used in construction of the coil. To determine the coil volume, the first step is to look at the magnitude of the force produced by a current I in a wire of length L_w in a magnetic field B

$$|F_{LM}| = |I|L_w B. \tag{23}$$

The time-averaged power generated by the force F_{LM} is

$$<\dot{W}_{PV}> = 1/2 F_{LM}\cdot\dot{z} = (\pi/2) fs\,|F_{LM}|s\cos\theta. \tag{24}$$

When Eq. (23) is substituted into Eq. (24) the power output becomes

$$<\dot{W}_{PV}> = \pi/2(|I|L_w B) fs\cos\theta. \tag{25}$$

The volume of wire in the coil is $V_w=L_w A_w=pV_c$, where p is the packing fraction of copper in the total coil volume V_c. Solving this for L_w and substituting L_w into Eq. (25) gives

$$<\dot{W}_{PV}> = \frac{\pi|I|pV_c Bfs\cos\theta}{2A_w} = \frac{\pi}{2}|j|pV_c Bfs\cos\theta, \tag{26}$$

where j is defined as the current density $j=I/A_w$. Equation (26) can now be solved for V_c,

$$V_c = \frac{2<\dot{W}_{PV}>}{\pi|j|pBfs\cos\theta} \tag{27}$$

Because j is not a specified parameter, we express it in terms of known quantities. The time-averaged Joule heating in the coil for an oscillating current is

$$<\dot{Q}_j> = \frac{|I|^2\rho L_w}{2A_w}. \tag{28}$$

The value used for the resistivity ρ of the wire must reflect the increase in temperature of the coil due to Joule heating. The current density is now calculated in terms of known quantities by dividing Eq. (28) by Eq. (26) and solving for $|j|$,

$$|j| = \frac{(<\dot{Q}_j>/<\dot{W}_{PV}>)\pi Bfs\cos\theta}{\rho}, \tag{29}$$

where $<\dot{Q}_j>/<\dot{W}_{PV}>$ is the fraction of power lost to Joule heating. The current density in Eq. (29) can be used to determine the wire size for the available current. The coil volume can now be determined by substituting Eq. (29) into Eq. (27),

$$V_c = \frac{2\rho<\dot{W}_{PV}>}{\pi^2 pB^2 f^2 s^2(<\dot{Q}_j>/<\dot{W}_{PV}>)\cos^2\theta}. \tag{30}$$

The coil volume in Eq. (30) is valid for both the axial and radial magnet configurations, but only for the short coil where the coil volume is in the magnetic field during the entire stroke.

Once the coil volume is known, the magnetic circuit, which includes the permanent magnet, air gap, and return iron, is designed. The short-coil, radial magnet will be discussed in this paper; similar steps can be used for the other cases. The volume of the air gap is the volume of the coil including clearance between the pole pieces and the coil plus the swept volume of the coil during the stroke. Since this volume is dependent on the final geometry of the magnetic circuit, a guess is made as to how much larger the air gap volume must be compared to the coil volume. Then the circuit is designed for this gap volume and it is determined if the coil will remain in the gap during the entire stroke. If the coil leaves the gap or the gap is too long, a new guess is made for the gap volume and the steps given below are repeated until the coil just remains within the gap during the entire stroke. Figure 4 shows the geometry of both a radial and axial magnetic circuit and defines the geometry variables. The only difference in the

magnetic circuit geometry between the long coil and short coil designs is the added length of the stroke to the return iron in the long coil, radial design. The first step in designing the magnetic circuit is to guess the ratio of gap volume to coil volume b_g then find the gap volume,

$$V_g = b_g V_c. \tag{31}$$

Next the volume of magnet can be determined from[6]

$$V_m = \frac{c_m B^2 V_g}{(BH)_{\max}}, \tag{32}$$

where $(BH)_{max}$ is the maximum energy product of the magnetic material and c_m is a scaling factor used to account for magnetic losses due to the iron and fringing effects. Equation (32) gives the minimum volume of magnetic material needed to achieve the desired magnetic field in the air gap. Now it is necessary to decide on the length L_g of the air gap. This value is picked by the designer and the calculation should be done for a number of different values to see its effect on the magnetic circuit size and weight. Small values of L_g are better for heat transfer of the Joule heating produced in the coil. The optimum length L_m of the magnet can now be calculated by

$$L_m = \frac{b_m B L_g}{H_m}, \tag{33}$$

where b_m is a scaling factor used to account for imperfections in the magnetic circuit and H_m is the demagnetizing force in the magnet at the operating point. To minimize the amount of magnet material the operating point is taken at $(BH)_{max}$ for the permanent magnet material selected. The largest $(BH)_{max}$ values are currently obtained with NdBFe permanent magnets. The cross-sectional area of the magnet perpendicular to the field is $A_m=V_m/L_m$. Similarly the cross-sectional area of the gap is $A_g=V_g/L_g$. Next the cross-sectional area of the return iron can be determined by $A_i=(B/B_i)A_g$, where A_i is the cross-sectional area of iron needed to keep the magnetic field in the return iron from saturating, and B_i is the maximum allowed magnetic field to keep from saturating the iron. Now the inner diameter of the magnet and air gap can be calculated using a center hole of specified size for the piston shaft and by using the cross-sectional area of the iron,

$$D_{im} = D_{ig} = \sqrt{4(A_i+A_s)/\pi}, \tag{34}$$

where A_s is the cross-sectional area of the hole needed for the shaft and D_{ig} is the inner diameter of the air gap, defined in Figure 4. The inner diameter of the air gap is placed at the smallest allowable diameter to reduce the extra volume introduced by the stroke of the piston. The extra

volume of the gap, due to the stroke, is dependent on the cross-sectional area of the gap. A larger gap cross-sectional area means a larger gap volume will be needed to contain the coil than would be needed if the gap cross-sectional area were smaller. This consideration also applies to the long coil design, a larger coil volume will be needed for larger diameter coils. Coils should be placed on the smallest possible diameter. The outer diameters of the magnet and air gap are given by

$$D_{om} = D_{im} + 2L_m; \quad D_{og} = D_{ig} + 2L_g. \tag{35}$$

Next the width w_m of the magnet can be determined by

$$w_m = \frac{4V_m}{\pi(D_{om}^2 - D_{im}^2)}. \tag{36}$$

The width w_g of the air gap, can be found using a similar equation. Since the length of the magnet will always be larger then the length of the air gap, the outer diameter D_{oi} of the iron can be found by

$$D_{oi} = \sqrt{D_{om}^2 + 4A_i/\pi}\ . \tag{37}$$

The inner diameter of the coil can be found by adding an appropriate clearance factor to the inner diameter of the air gap, while the outer diameter of the coil is found by subtracting a clearance factor from the outer diameter of the air gap. When deciding on the clearance factor for the inner diameter of the coil, allowance for the bobbin on which the wire is wrapped must be considered. Now that the diameters of the coil are known, the width w_c of the coil can be found using an equation similar to Eq. (36). The difference w_g - w_c should be the stroke of the piston. If this is not the case, a new b_g guess in Eq. (31) is made for the volume of the gap and the procedure is repeated until w_g - w_c= s. A similar procedure can be used for the short coil, axial magnet, by using the appropriate geometry. This procedure should be repeated for a number of different piston strokes to determine the effect of the stroke on the size and weight.

The long coil designs always have the entire magnetic field within the coil. The difference in coil volume between the short and long coil designs is that for the same joule heating loss, the current density must be lower for the long coil design since it contains more wire then the short coil. The fraction of the coil within the gap is $w_g/(w_g+s) = [1+(s/w_g)]^{-1}$. Thus Eq. (30) gives the volume of the coil within the gap if the relative Joule heating loss within this portion of the coil is also the same fraction of the total relative Joule heating loss ($<\dot{Q}_j>/<\dot{W}_{PV}>$). The total coil volume for the long coil design then becomes

$$V_c = \frac{2\rho<\dot{W}_{PV}>(1+s/w_g)^2}{\pi^2 pB^2 f^2 s^2 (<\dot{Q}_j>/<\dot{W}_{PV}>)\cos^2\theta}, \tag{38}$$

where w_g is the width of the gap as shown in Figure 4. Equation (38) is valid for any long coil case. Using Eq. (38) for the coil volume and a procedure similar to the one given above, the magnetic circuit can be designed for both long-coil cases. The major difference between the procedures for the short and long coil cases is that a initial guess must be made for the width of the gap in the long coil case and for the long coil cases, $w_g + s = w_c$ is used to determine if the solution is correct.

The constants c_m, b_m, and B_i, must be adjusted to make these equations agree with more accurate results calculated from finite element techniques. By using finite element software for magnetic circuits, the proper values of the constants can be determined for a wide range of geometries. The constants vary some-what with the geometry. Using a finite element package, the constants have been determined to be: c_m = 1.2 to 3, b_m = 1.2 to 1.8, B_i = 1 to 1.6 Tesla.

The efficiency of the linear motor is given by

$$\eta_m = <\dot{W}_{PV}>/\dot{W}_{input} = \frac{1}{(1 + <\dot{Q}_j>/<\dot{W}_{PV}> + <\dot{W}_g>/<\dot{W}_{PV}> + <\dot{W}_l>/<\dot{W}_{PV}>)}, \tag{39}$$

where $\dot{W}_{input}$ is the electrical input power and $<\dot{W}_l>$ represents all other losses not discussed previously. These other losses, such as windage and eddy current losses, are usually negligible. System size and weight are decreased by increasing the joule heating loss $<\dot{Q}_j>$, but that leads to lower efficiency. A good compromise for satellite applications often gives $<\dot{Q}_j>/<\dot{W}_{PV}>$ = 0.1 to 0.2 and $<\dot{W}_g>/<\dot{W}_{PV}>$ = 0.02 to 0.05. Motor efficiencies of 75% to 85% are typical.

Advantages and Disadvantages of the Different Magnetic and Coil Configurations

Long coil designs require more coil volume but a smaller air gap volume, giving an overall savings on system weight at the expense of adding to the amount of mass that must be moved. This is an advantage to smaller systems that must normally add additional moving mass to operate at the desired resonant frequency. Comparing Eq. (38) to Eq. (30) shows that the long coil volume is larger than the short coil volume by the factor $[1+(s/w_g)]^2$. Typical values of s/w_g vary from 0.5 to 1 so that the long coil volume varies from 2 to 4 times the short coil volume. The magnet and iron weight of the long-coil configuration will be about 40% to 70% of that for

the short-coil configuration. The outer diameter of the long-coil configuration will be about 80% to 90% of that for the short-coil configuration. Long coils use more potting compound and outgas more than short coils. A portion of the wire in the long coils experiences a magnetic field that varies from zero to the value in the air gap. The eddy currents induced within the wire diameter will lead to an additional heating effect that is on the order of 1% of the PV power.

Radial magnet configurations offer reduced system weight and size compared to axial magnet configurations. System weight for radial magnet configurations will be 50% to 70% of that for the axial magnet configurations. The outer diameter of radial magnet configurations will be 60% to 70% of that for axial magnet configurations. The cost of a radial magnet will be more then the axial magnet since radial magnets must be made in segments in order to be magnetized in the radial direction. If a radial magnet is designed properly, the epoxy used during assembly can be removed after the magnet is assembled.

Flexure Spring

Flexure spring bearings are used in place of traditional sliding bearings. They have the advantage of not having rubbing parts to wear out and contaminate the fluid. Flexure springs are constructed of a thin material having a high ratio of fatigue stress limit to Young's modulus. Stainless steel or beryllium copper are good candidates for such a material. The springs are designed to have a high radial stiffness and a low axial stiffness. This allows the clearance seal to maintain its close alignment while increasing the moving mass only a small amount due to k_z in Eq. (13). The desired radial stiffness k_r of the flexure springs in normal gravity is

$$k_r = \frac{mg}{C_r t_g}, \tag{40}$$

where g is the gravitational constant and C_r is the ratio of allowable radial displacement to the clearance gap thickness. The value of C_r should usually be about 0.5 or less to prevent channeling from occurring in the clearance gap that will cause an increase in the power loss. The desired axial spring stiffness is expressed as

$$k_z = 4C_z\pi^2 mf^2, \tag{41}$$

where C_z is the ratio of axial spring force to the inertial force. From a practical standpoint, C_z should not be less than about 15% or instability of the system may result when dual-opposed configurations are used. Values higher than 25% begin to significantly increase the moving mass. The desired ratio of radial to axial spring stiffness is then given by

$$\frac{k_r}{k_z} = \frac{g}{4\pi^2 C_r C_z t_g f^2} \tag{42}$$

As an example for $C_r = C_z = 0.20$, and $t_g = 15$ μm, then $k_r/k_z = 460$ at $f = 30$ Hz and $k_r/k_z = 204$ at $f = 45$ Hz. Because there may be large gas side forces associated with slight axial misalignment, the actual value of C_r should be much less than 0.20 to prevent any possible contact during operation.

The Oxford-style flexure spring,[2] shown in Figure 5a, has been used for several years for small compressors. A problem with the Oxford spring is the highly localized stress concentration that occurs around the holes at the end of the photoetched slots. These stress concentrations occur because the flexing arms project out from the clamped region at an angle much different than 90°. As a result, in order to keep the peak stress below the maximum allowable stress for infinite fatigue life, the flexing arm has to be made quite long. Hence, the need for a spiral of at least a whole turn. The long flexing arm greatly reduces the radial stiffness. With properly shaped clamp rings, the flexing arms of the Oxford spring could project away from the clamp at nearly 90° and reduce this stress concentration. The arm length can then be reduced, leading to a greater radial stiffness while still keeping the peak stress below the allowable stress. Figure 5b shows the result of such a modification similar to that proposed by Wong et al.[7]. By

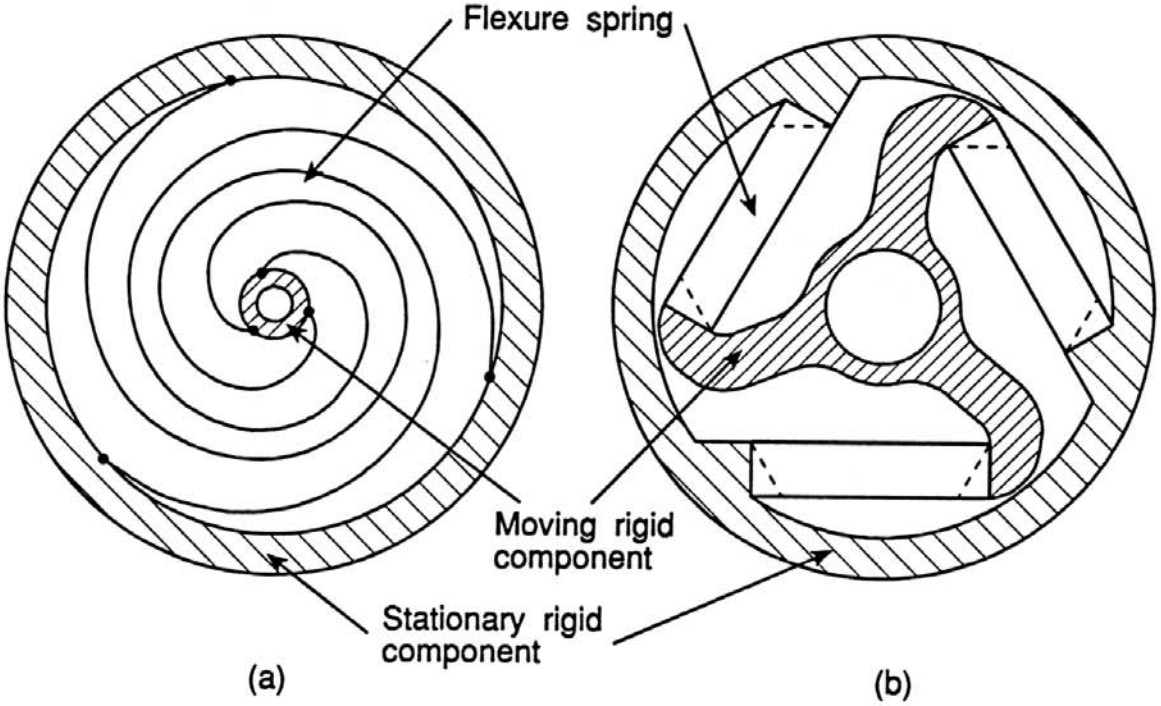

Figure 5. (a) Oxford flexure spring, (b) Linear flexure spring.

connecting the flexing arm to the moving rigid component at the maximum possible radius, the axial rotation is reduced although it adds additional mass to the moving component. The center hole for the shaft can be as much as 25% of the outer diameter of the spring, which allows for stiffer shafts with the same mass. Because of the axial rotation, the stress concentrations are minimized by having the clamped edge along the dashed lines in Figure 5b. For the sake of simplicity the following analyses of the spring ignore this effect and use a clamped edge shown by the solid lines in Fig. 5b.

Accurate calculations of stiffness and stresses in these springs can only be done with nonlinear finite element techniques. The straight arms of the linear flexure spring are more amenable to simple analytical calculations which help scaling the flexure springs to different sizes and serve as a good starting point for detailed design. By using simple beam analysis for a cantilever beam with both ends clamped, the maximum stress is found to be

$$\sigma_{max} = 3E(s/2)t_s/L_s^2, \tag{43}$$

where E is Young's modulus, t_s is the spring thickness, and L_s is the spring length. A large ratio, σ_{max}/E, allows for larger strokes. The axial and radial stiffnesses are

$$k_z = 3N_sEw_st_s^3/L_s^3 \tag{44}$$

$$k_r = 3N_sEt_sw_s^3G(s/L_s)/L_s^3, \tag{45}$$

where w_s is the width of the spring arm, N_s is the number of springs, and the factor of 3 comes from the 3 arms of the spring. G is a function of (s/L_s) and is included to account for the decrease in radial stiffness with axial displacement. It has the property of $G(0)=1$. This function can be determined only from a finite element analysis of a particular spring design. The radial stiffness decreases rapidly as the axial displacement increases and at full displacement may be at least an order of magnitude less than that at zero displacement. Equation (45) is a poor fit to the finite element analysis performed on the linear spring. A better fit is achieved if it is assumed that one spring arm acts in pure tension to provide the radial stiffness which results in

$$k_r = N_sEt_sw_sG(s/L_s)/L_s. \tag{46}$$

The ratio of stiffness is given by

$$k_r/k_z = (L_s/t_s)^2G(s/L_s)/3. \tag{47}$$

The required number of springs is found by comparing Eq. (44) with Eq. (41) to arrive at

$$N_s = \frac{4\pi^2 C_z m f^2 L_s^3}{3E w_s t_s^3}. \tag{48}$$

The resultant C_r from Eqs. (46) and (40) should be less than some established value such as 0.2. The desired number of springs will be in the range of 5 to 15 for most compressors. A thin spring (low t_s) leads to low stresses according to Eq. (43), high radial to axial stiffness ratio according to Eq. (47), but a large number of springs according to Eq. (48).

In the Linear design the spring length and inner diameter of the outer clamp ring are related by

$$L_s \approx D_s/2, \tag{49}$$

where D_s is the inner diameter of the outer clamp ring. Likewise, the spring width is

$$w_s \approx D_s/5. \tag{50}$$

Thus, Eqs. (43) through (47) become

$$\sigma_{max} \approx 6Est_s/D_s^2, \tag{51}$$

$$k_z \approx 3N_s(8/5)Et_s^3/D_s^2, \tag{52}$$

$$k_r \approx N_s(2/5)Et_s G(s/D_s), \tag{53}$$

$$k_r/k_z \approx (D_s/t_s)^2 G(s/D_s)/12. \tag{54}$$

Using Eq. (51) to solve for t_s in terms of the maximum allowed stress, Eq. (54) can be expressed in the alternate form

$$k_r/k_z = \frac{3(s/D_s)^2 G(s/D_s)}{(\sigma_{max}/E)^2}, \tag{55}$$

and Eq. (48) for the linear spring design can be expressed as

$$N_s \approx \frac{180\pi^2 C_z m f^2 (s/D_s)^3}{E(\sigma_{max}/E)^3 D_s}. \tag{56}$$

For most spring designs the product $(s/D_s)^2 G(s/D_s)$ is an increasing function of s/D. Thus, according to Eq. (55) a high k_r/k_z is obtained by making s/D_s as large as possible. But according to Eq. (56) a large s/D_s leads to a large number of springs. A compromise is then needed. Typical s/D_s values range from about 0.10 to 0.15. Equation (56) also shows that D_s should be made as large as possible to reduce the number of springs. In practice the maximum D_s will be

about that of the magnet outer diameter D_{om}. The stroke should then be made as large as possible for a desired number of springs to maximize k_r/k_z and to minimize V_c and the resulting linear motor size and mass according to Eq. (30). We can express s in terms of N_s and D_s by first using Eqs. (48), (49), and (50) to solve for t_s in terms of N_s and D_s. This t_s is then substituted into Eq. (51) to obtain

$$s = \frac{(\sigma_{max}/E)}{6}\left[\frac{ED_s^4N_s}{(5/6)\pi^2C_zmf^2}\right]^{1/3}. \tag{57}$$

Substituting this equation into Eq. (55) gives

$$k_r/k_z = \left[\frac{ED_sN_s}{(5/6)\pi^2C_zmf^2}\right]^{2/3}\frac{G(s/D_s)}{12}. \tag{58}$$

A material with the largest possible value of $E^{1/3}(\sigma_{max}/E)$ is desirable to increase the stroke and a large E is desirable to increase k_r/k_z. Thus, stainless steel is better than beryllium copper from both standpoints. Because D_s is related to the motor diameter, and the motor diameter was found originally by assuming a given value for the stroke, an iterative procedure must be used to find a consistent set of s, m, and D_s values that minimize the motor size and weight, yet provides the necessary k_r/k_z to prevent contact between the piston and cylinder.

SCALING LAWS

The set of equations developed in the previous section can be used for the original design of a flexure spring compressor. Finite element analysis is required for the calculation of the flexure spring radial stiffness and for more accurate values of the other spring parameters. It is also needed for more accurate sizing of the magnets and return iron in the linear motor. Calculations with finite element software can be time consuming since many trial and error calculations are required. These design equations minimize the amount of trial and error calculations necessary. Once a detailed design is developed for one size compressor, any other size can be quickly designed if the correct scaling laws are known. Two cases will be considered. The simpler case is that in which the frequency is allowed to vary as the size changes. That case is treated first and the case of constant frequency will be addressed later.

Variable Frequency

Let K be some constant which is used to form the scaling variable for the various dimensions and

the frequency. The base design corresponds to K=1, whereas an increase in size utilizes K>1 and a decrease in size utilizes K<1. The scale factor for each parameter will be some power of K. For the case of a variable frequency, use the following scaling laws:

frequency,	$f \propto 1/K$	magnet inner diameter,	$D_{im} \propto K$
stroke,	$s \propto K$	magnet outer diameter,	$D_{om} \propto K$
piston diameter,	$D \propto K^{3/2}$	magnet width,	$w_m \propto K$
piston length,	$L_p \propto K^{3/2}$	spring diameter,	$D_s \propto K$
coil inner diameter,	$D_{ic} \propto K$	spring thickness,	$t_s \propto K$
coil outer diameter,	$D_{oc} \propto K$	number of springs,	$N_s \propto K$.
coil width,	$w_c \propto K$		

The parameters P_0, P_r, $(\langle \dot{Q}_f \rangle / \langle \dot{W}_{PV} \rangle)$, p, B, $(BH)_{max}$, ϕ, and θ remain constant. Using the relevant design equation, the scaling factors for various related parameters are obtained. The selection of scale factors given above must satisfy the consistency equation that relates the coil dimensions to the compression space parameter, Eq. (30). This is shown in line 1 of Table 1. Scale factors for various performance parameters are given in lines 2 to 14 of Table 1. The terms $|j|$, k_r/k_z, and σ_{max} are independent of the scale factor which is the ideal case. However, the relative deflections, lines 13 and 14, vary as K instead of being independent of K. Thus, these parameters place an upper limit on K, which depends on the initial values of $\Delta R/t_g$ and $\Delta z/s$. All values of K below 1 would be permitted although too small values of K lead to unacceptably high frequencies. Lines 9 to 12 show a scale factor of K^3 for all the force terms. Thus, their relative magnitudes will not change, which is desirable.

The scale factors for this case are particularly desirable since all the spring and linear motor dimensions vary as K. As a result there is no need for recalculations with finite element software for either of those two complex components. Because of the limitations associated with the non-ideal scale factor for the relative deflections as well as with the number of springs, this case is best used for size reductions rather than size increases.

Constant Frequency

A good (but not necessarily exclusive) set of scale factors for this case is as follows:

frequency,	$f \propto K^0$	magnet inner diameter,	$D_{im} \propto K$
stroke,	$s \propto K^{1/2}$	magnet outer diameter,	$D_{om} \propto K$

piston diameter,	$D \propto K^{3/2}$	magnet width,	$w_m \propto K^{1/2}$
piston length,	$L_p \propto K$	spring diameter,	$D_s \propto K$
coil inner diameter,	$D_{ic} \propto K$	spring thickness,	$t_s \propto K^{3/2}$
coil outer diameter,	$D_{oc} \propto K$	number of springs,	$N_s \propto K^0$.
coil width,	$w_c \propto K^{1/2}$		

The resulting performance scale factors are shown in Table 1 for the constant frequency case. As shown in line 1, the selection is consistent and all terms of the force balance have the same scale factor. Non-ideal scale factors occur for $|j|$, k_r/k_z, and $\Delta z/s$. However, for the spring $s/D_s \propto 1/K^{1/2}$ in this case, which means that for large K the smaller s/D_s will contribute to a greater radial stiffness from the $G(s/D_s)$ factor that counteracts the $1/K$ dependence predicted from simple beam theory. Likewise, the larger $\Delta z/s$ at low K will also be compensated because of the larger s/D_s. The variable current density does not present any inherent problems as long as K is not

Table 1. Scale factors for derived compressor parameters.

Line #	Eq. #	Parameter	Proportionality	Scale Factor	
				variable f	constant f
1	30	Coil volume	$V_c \propto \langle \dot{W}_{PV} \rangle / (f^2 s^2)$ $w_c(D_{oc}^2 - D_{ic}^2)$ and $D^2/(fs)$	consistency K^3 & K^3	consistency $K^{5/2}$ & $K^{5/2}$
2	18	Power	$\langle \dot{W}_{PV} \rangle \propto fsD^2$	K^3	$K^{7/2}$
3	29	Current density	$\|j\| \propto fs$	K^0 (ideal K^0)	$K^{1/2}$
4	22	Clearance gap	$t_g \propto [L_p fsD]^{1/3}$	K	K
5	46	Radial stiffness	$k_r \propto N_s t_s w_s / D_s$	K^2	$K^{3/2}$
6	44	Axial stiffness	$k_z \propto N_s w_s t_s^3 / D_s^3$	K^2	$K^{5/2}$
7	47	Radial/Axial stiffness	$k_r/k_z \propto (D_s/t_s)^2$	K^0 (ideal K^0)	$1/K$ (ideal K^0)
8	43	Maximum spring stress	$\sigma_{max} \propto t_s s / D_s^2$	K^0 (ideal K^0)	K^0 (ideal K^0)
9	8	Force balance (flexure spring)	$1/2 k_z s \propto N_s t_s w_s^3 s / D_s^3$	K^3	K^3
10	8	Force balance (gap spring)	$PA\cos\phi \propto D^2$	K^3	K^3
11	8	Force balance (inertia)	$2\pi^2 f^2 sm \propto f^2 sm$	K^3 (for $m \propto K^4$)	K^3 (for $m \propto K^{5/2}$)
12	8	Force balance (motor force)	$F_{LM} \sin\theta \propto D^2$	K^3	K^3
13	40	Relative radial deflection	$C_r = \Delta R / t_g \propto m/(k_r t_g)$	K (ideal K^0)	K^0 (ideal K^0)
14	-	Relative axial deflection	$\Delta z/s \propto m/(k_z s)$	K (ideal K^0)	$1/K^{1/2}$ (ideal K^0)

much larger than 1. This set of scaling laws is estimated to be good over the range of $0.25 \le K \le 2.0$. With a baseline design of $\langle \dot{W}_{PV} \rangle$ = 350 W, these scale factors are good for the range of $\langle \dot{W}_{PV} \rangle$ between 3 W and 4 kW. Because the stroke and spring dimensions have different scale factors, a finite element analysis of the new spring will be necessary in this case. Likewise the different scale factors for the coil width and the coil diameters may require a new finite element analysis of the magnet and iron assembly to be certain of the magnetic field in the air gap of the new design. For $K>2$, the ratio $D/D_{oc} \propto K^{1/2}$ may cause the piston diameter to become relatively large compared with the coil outer diameter.

CONCLUSIONS

A set of design equations has been derived to determine the optimum geometry (minimum size and mass) for a linear compressor using flexure springs. Input variables are desired performance parameters such as compressor PV power, frequency, average pressure, pressure ratio, pressure-to-volume phase angle, and compressor efficiency. The set of equations derived here easily show how these performance parameters affect the compressor design. These equations need to be supplemented by finite element calculations for the accurate and detailed design of the magnet system and the flexure springs. The equations were used to develop a set of scaling laws of the compressor system that is useful for changing the size of a previously designed compressor with a minimum number of design changes. These scaling laws should be valid over at least the range of 3 W to 4 kW of compressor PV power.

NOMENCLATURE

A	cross-sectional area of the piston	C_r	ratio of radial displacement to clearance gap length
A_g	cross-sectional area of air gap	C_z	ratio of axial spring force to inertial force
A_i	cross-sectional area of return iron	D	diameter of piston
A_m	cross-sectional area of magnet	D_s	inner diameter of outer clamp ring for flexure spring
A_s	cross-sectional area of piston shaft	E	Young's modulus
A_w	cross-sectional area of coil wire	f	operating frequency
b	coefficient of viscous drag	F_{LM}	motor force
B	magnetic field in air gap	g	gravitational constant
B_i	maximum magnetic field in iron	H_m	demagnetizing force in the magnet at the operating point
b_g	ratio of air gap to coil volume	i	$(-1)^{1/2}$
$(BH)_{max}$	maximum energy product of magnetic material	I	wire current
b_m	scaling factor for imperfections in the magnetic circuit		
C_m	scaling factor for magnetic losses		

k_r	total radial spring constant of flexure springs
k_z	total axial spring constant of flexure springs
j	current density (I/A_w)
L_{cg}	length of the clearance seal
L_g	length of air gap
L_m	length of magnet
L_s	length of spring arm
L_w	length of wire in coil
m	mass of the piston assembly
N_s	number of flexure springs
p	packing fraction (V_w/V_c)
P	instantaneous pressure
P_0	average system pressure
P_1	amplitude of the dynamic pressure in the compression space
P_{B1}	amplitude of the dynamic pressure in the bounce space
P_r	pressure ratio (maximum pressure / minimum pressure)
ΔP	pressure drop through clearance seal
$<\dot{Q}_j>$	time-averaged joule heating in coil
R	coil wire total resistance
s	stroke of piston
t_g	thickness of clearance gap
t_s	flexure spring thickness
V_c	coil volume
$\dot{V}_{cg}$	volumetric flow rate through the clearance gap
V_{co}	compressor swept volume ($V_{co}= sA$)
$\dot{V}_{co}$	volumetric flow rate in compressor
V_g	air gap volume
V_m	permanent magnet volume
V_w	wire volume (L_wA_w)
w	width of the clearance seal ($w=\pi D$ for an annular gap)
w_c	width of coil
w_g	width of air gap
w_m	width of magnet
$<\dot{W}_g>$	compressor power lost to flow through the clearance gap
$\dot{W}_{PV}$	instantaneous compressor PV power
$<\dot{W}_{PV}>$	time-averaged compressor PV power
w_s	width of spring arm
z	spacial position of the piston
$\dot{z}$	piston velocity
$\ddot{z}$	acceleration of the piston
Z_f	flow impedance
β	phase angle between piston position and $-P_B$
η_m	compressor efficiency
θ	angle between the motor force and the imaginary axis
μ	working fluid dynamic viscosity
ρ	wire material resistivity
ω	angular frequency, $\omega=2\pi f$
ϕ	phase angle between the position and dynamic pressure

REFERENCES

1. C. D. Zafiratos, in: Physics, John Wiley & Sons, New York (1985).
2. G. Davey, "Review of the Oxford Cryocooler", in: Advances in Cryogenic Engineering, vol. 35B, R.W. Fast, ed., Plenum Press, New York (1990), p. 1423.
3. S. E. Schwarz and W. G. Oldham, in: Electrical Engineering, Holt, Rinehart and Winston, New York (1984).
4. R. M. Olson, in: Essential of Engineering Fluid Mechanics, Harper & Row, New York, New York (1980).
5. P. J. Kerney, "Linear Drive Stirling Cooler Technology", in: Applications of Cryogenic Technology, vol 10, J. P. Kelley, ed., Plenum Press, New York (1991), p. 15.
6. L. R. Moskowitz, in: Permanent Magnet Design and Application Handbook, Krieger, Malabar, Florida (1976).
7. Wong, Pan, and Johnson, "Novel Linear Flexure Bearing", in: Proceedings of the 7th International Cryocooler Conference, this publication (1993).